Going back to the start: do cancer and haematological disorders affect germ cells in prepubertal boys?

Characterisation of the neonatal brain using myelin-sensitive magnetisation transfer imaging

Manuel Blesa Cábez[a,1,*], Kadi Vaher[a,*], Elizabeth N. York[b,c,d], Paola Galdi[d], Gemma Sullivan[a], David Q. Stoye[a], Jill Hall[a], Amy E. Corrigan[e], Alan J. Quigley[e], Adam D. Waldman[b,d], Mark E. Bastin[b,d], Michael J. Thrippleton[b,d], James P. Boardman[a,b]

Author affiliations

[a]MRC Centre for Reproductive Health, Institute for Regeneration and Repair, University of Edinburgh, Edinburgh BioQuarter, EH16 4UU

[b]Centre for Clinical Brain Sciences, University of Edinburgh, Edinburgh, EH16 4SB, UK

[c]Anne Rowling Regenerative Neurology Clinic, Edinburgh, EH16 4SB, UK

[d]Edinburgh Imaging, University of Edinburgh, Edinburgh, UK

[e]Royal Hospital for Children & Young People, Edinburgh, EH16 4TJ, UK

[1]Corresponding author: Manuel Blesa Cábez, Chancellor's Building, 49 Little France Crescent, Edinburgh BioQuarter, Edinburgh EH16 4SB, UK. Email: manuel.blesa@ed.ac.uk

*These authors contributed equally to the work.

Abstract

A cardinal feature of the encephalopathy of prematurity is dysmaturation of developing white matter and subsequent hypomyelination. Magnetisation transfer imaging (MTI) offers surrogate markers for myelination including magnetisation transfer ratio (MTR) and magnetisation transfer saturation (MTsat). Using data from 105 neonates, we characterise MTR and MTsat in the developing brain and investigate how these markers are affected by gestational age at scan and preterm birth. We explore correlations of the two measures with fractional anisotropy (FA), radial diffusivity (RD) and T1w/T2w ratio which are commonly used markers of white matter integrity in early life. We used two complementary analysis methods: voxel-wise analysis across the white matter skeleton, and tract-of-interest analysis across 16 major white matter tracts. We found that MTR and MTsat positively correlate with gestational age at scan. Preterm infants at term-equivalent age had lower values of MTsat in the genu and splenium of the corpus callosum, while MTR was higher in central white matter regions, the corticospinal tract and the uncinate fasciculus. Correlations of MTI metrics with other MRI parameters revealed that there were moderate positive correlations between T1w/T2w and MTsat and MTR at voxel-level, but at tract-level FA had stronger positive correlations with these metrics. RD had the strongest correlations with MTI metrics, particularly with MTsat in major white matter tracts. The observed changes in MTI metrics are consistent with an increase in myelin density during early postnatal life, and lower myelination and cellular/axonal density in preterm infants at term-equivalent age compared to term controls. Furthermore, correlations between MTI-derived features and conventional measures from dMRI provide new understanding about the contribution of myelination to non-specific imaging metrics that are often used to characterise early brain development.

Keywords: magnetisation transfer, preterm birth, neonate, white matter, myelin

1 Abbreviations

AF	arcuate fasciculus
ATR	anterior thalamic radiation
CC genu	corpus callosum genu/forceps minor
CC splenium	corpus callosum splenium/forceps major
CCG	cingulum cingulate gyrus
CST	corticospinal tract
dHCP	developing human connectome project
dMRI	diffusion magnetic resonance imaging
FA	fractional anisotropy
FDR	false discovery rate
FWER	family-wise error correction
GA	gestational age
GM	grey matter
IFOF	inferior fronto -occipital fasciculus
ILF	inferior longitudinal fasciculus
MPF	macromolecular proton fraction
MRI	magnetic resonance imaging
MTI	magnetisation transfer imaging
MTR	magnetisation transfer ratio
MTsat	magnetisation transfer saturation
R1app	approximation of R1
RD	radial diffusivity
ROI	region of interest
SNR	signal-to-noise ratio
TE	echo time
TEA	term-equivalent age
TFCE	threshold-free cluster enhancement
TR	repetition time
UNC	uncinate fasciculus
WM	white matter

2

1 Introduction

The integrity of brain development during pregnancy and the new born period is critical for life-long cognitive function and brain health. During the second and third trimesters of pregnancy, there is a phase of rapid brain maturation characterised by volumetric growth, increases in cortical complexity, white matter (WM) organisation and myelination (Counsell et al., 2019; Dubois et al., 2021). Early exposure to extrauterine life due to preterm birth, defined as birth < 37 weeks of gestation, affects around 11% of births and is closely associated with neurodevelopmental, cognitive and psychiatric impairment (Johnson and Marlow, 2017; Nosarti et al., 2012; Wolke et al., 2019), and alterations to brain development that are apparent using MRI (Boardman and Counsell, 2019; Counsell et al., 2019; Pecheva et al., 2018).

Structural MRI (T1- and T2-weighted) and diffusion MRI (dMRI) have revealed a phenotype of preterm birth that includes changes in global and regional tissue volumes and cortical complexity, and altered microstructural integrity of the WM (Counsell et al., 2019; Pecheva et al., 2018). These imaging features capture the encephalopathy of prematurity (EoP), which is thought to underlie long term impairments (Volpe, 2009). Diffusion metrics are influenced by microstructural properties of the underlying tissue including axonal density and diameter, and water content; although myelination may alter/contribute to water diffusivity, myelin does not directly contribute to the diffusion signal due to short T2 (Mancini et al., 2020; van der Weijden et al., 2020).

Pre-oligodendrocytes are particularly vulnerable to hypoxia-ischaemia and inflammation associated with preterm birth (Back and Volpe, 2018; Volpe et al., 2011). Although this cell population is mostly replenished following primary injury, subsequent differentiation into myelin-producing oligodendrocytes can fail, leading to hypomyelination (Billiards et al., 2008; Volpe, 2019). Therefore, imaging tools that more specifically model myelination in early life could enhance biology-informed assessment of EoP.

Several MRI techniques are sensitive to myelin content (Lazari and Lipp, 2021; Mancini et al., 2020; Piredda et al., 2021). In the developing brain, the most commonly applied myelin-sensitive imaging techniques are those based on relaxometry, such as T1 (or its inverse, R1) or T2 (or its inverse, R2) mapping (e.g. Counsell et al., 2003; Grotheer et al., 2022; Kulikova et al., 2015; Leppert et al., 2009; Maitre et al., 2014; Schneider et al., 2016), quantification of myelin water fraction (e.g. Dean et al., 2014; Deoni et al., 2011; Melbourne et al., 2013), and calculation of T1w/T2w ratio (e.g. Filimonova et al., 2023; Grotheer et al., 2023; Lee et al., 2015; Soun et al., 2017). However, T1 and T2 relaxation are partly determined by iron concentration (Birkl et al., 2019; Stüber et al., 2014), and T1w/T2w ratio correlations with other myelin-sensitive MRI parameters and histological myelin measurements are low (Arshad et al., 2017; Sandrone et al., 2023; Uddin et al., 2018).

Magnetisation transfer imaging (MTI) is a family of MRI techniques sensitive to subtle pathological changes in tissue microstructure which cannot typically be quantified with conventional MRI (Sled, 2018). MTI is based on the exchange of magnetisation between immobile protons associated with macromolecules, and mobile protons in free water. MTI is sensitive to myelin-associated macromolecules such as cholesterol, myelin basic protein, sphingomyelin and galactocerebrosides, and thus it provides a surrogate marker of myelin integrity (Mancini et al., 2020). To date, MTI has mainly been used to study demyelinating diseases such as multiple sclerosis (Sled, 2018; York et al., 2022b).

Magnetisation transfer ratio (MTR), calculated as the percentage change in signal with and without off-resonance radiofrequency saturation, is the most widely used MTI metric. MTR is, however, susceptible to transmit ($B1^+$) field inhomogeneities (Helms et al., 2010a), and T1 relaxation effects, and varies widely depending upon specific acquisition parameters (Samson et al., 2006; York et al., 2022c). Biological interpretation of MTR is therefore challenging, which presents a barrier to clinical translation. The addition of a T1w sequence allows computation of magnetisation transfer saturation (MTsat) which inherently corrects for $B1^+$ inhomogeneities and T1 relaxation to a substantial degree (Helms et al., 2008b; Samson et al., 2006). MTsat hence addresses some limitations of MTR within clinically feasible acquisition times and the resulting parametric maps have visibly better tissue contrast compared with MTR (Helms et al., 2008b; Samson et al., 2006; York et al., 2022b). Higher values of MTR and MTsat are associated with greater myelin density.

In neonates, MTR has been used to characterise brain development during the preterm period from birth up to term-equivalent age (TEA): in general, MTR values in WM increase with gestational age (GA) at scan (Nossin-Manor et al., 2015, 2013, 2012; Zheng et al., 2016). In addition, at the age of 4 years, children born very preterm have lower MTR values across the WM compared to term-born peers, and WM MTR positively correlates with language and visuo-motor skills (Vandewouw et al., 2019). Furthermore, in infancy, an MTI-derived macromolecular proton fraction (MPF) has predictive value for neurocognitive outcomes (Corrigan et al., 2022; Zhao et al., 2022). Yet, the use of MTI in the neonatal brain has been scarce, and, to the best of our knowledge, MTsat has not been used to study myelination in human neonates. Furthermore, no studies have explored the effect of preterm birth on MTI metrics in comparison to term controls at TEA.

In this work, we aimed to obtain a description of brain myelination processes by applying MTI in the neonatal period. We had three objectives: 1) to characterise the associations of MTsat and MTR in neonatal WM with GA at MRI scan; 2) to test the hypothesis that myelin-sensitive features would differ between preterm infants at TEA and term controls; and 3) to assess the relationship between MTI metrics and the T1w/T2w ratio, a commonly used myelin proxy, fractional anisotropy (FA), which is most robustly associated with EoP but is not specific to myelination, and radial diffusivity (RD), a diffusion biomarker that has been related to myelin pathologies (Lazari and Lipp, 2021; Mancini et al., 2020; Song et al., 2002).

2 Material and methods

2.1 Participants and data acquisition

Participants were very preterm infants (GA at birth < 32 completed weeks) and term-born controls recruited as part of a longitudinal study designed to investigate the effects of preterm birth on brain structure and long-term outcome (Boardman et al., 2020). The cohort exclusion criteria were major congenital malformations, chromosomal abnormalities, congenital infection, overt parenchymal lesions (cystic periventricular leukomalacia, haemorrhagic parenchymal infarction) or post-haemorrhagic ventricular dilatation. The study was conducted according to the principles of the Declaration of Helsinki, and ethical approval was obtained from the UK National Research Ethics Service. Parents provided written informed consent. 105 neonates (83 preterm and 22 term) who underwent MTI at TEA at the Edinburgh Imaging Facility (Royal Infirmary of Edinburgh, University of Edinburgh, UK) were included in the current study.

A Siemens MAGNETOM Prisma 3 T clinical MRI system (Siemens Healthineers, Erlangen, Germany) and 16-channel phased-array paediatric head coil were used to acquire a three dimensional (3D) T1w magnetisation prepared rapid gradient echo (MPRAGE) structural image (voxel size = 1 mm isotropic, echo time [TE] = 4.69 ms and repetition time [TR] = 1970 ms); 3D T2-weighted SPACE images (T2w) (voxel size = 1mm isotropic, TE = 409 ms and TR = 3200 ms) and axial dMRI data. dMRI volumes were acquired in two separate acquisitions to reduce the time needed to re-acquire any data lost to motion artifacts: the first acquisition consisted of 8 baseline volumes (b = 0 s/mm^2 [b0]) and 64 volumes with b = 750 s/mm^2; the second consisted of 8 b0, 3 volumes with b = 200 s/mm^2, 6 volumes with b = 500 s/mm^2 and 64 volumes with b = 2500 s/mm^2. An optimal angular coverage for the sampling scheme was applied (Caruyer et al., 2013). In addition, an acquisition of 3 b0 volumes with an inverse phase encoding direction was performed. All dMRI volumes were acquired using single-shot spin-echo echo planar imaging (EPI) with 2-fold simultaneous multi-slice and 2-fold in-plane parallel imaging acceleration and 2 mm isotropic voxels; all three diffusion acquisitions had the same parameters (TR/TE 3400/78.0 ms). MTI consisted of three sagittal 3D multi-echo spoiled gradient echo images (TE = 1.54/4.55/8.56 ms, 2 mm isotropic acquired resolution) magnetisation transfer (TR = 75 ms, flip angle = 5°, gaussian MT pulse (offset 1200 Hz, duration 9.984 ms, flip angle = 500°) [MT_{on}]), proton density-weighted (TR = 75 ms, flip angle = 5° [MT_{off}]) and T1w (TR = 15 ms, flip angle = 14° [MT_{T1w}]) acquisitions. All acquisitions affected by motion artifacts were re-acquired multiple times as required; dMRI acquisitions were repeated if signal loss was seen in 3 or more volumes. The full acquisition protocol can be found in the cohort manuscript (Boardman et al., 2020).

Infants were fed and wrapped and allowed to sleep naturally in the scanner. Pulse oximetry, electrocardiography and temperature were monitored. Flexible earplugs and neonatal

earmuffs (MiniMuffs, Natus) were used for acoustic protection. All scans were supervised by a doctor or nurse trained in neonatal resuscitation.

2.2 Data preprocessing

The image analysis was performed with MRtrix3 (Tournier et al., 2019), FSL 5.0.11 (Smith et al., 2004), ANTs (Avants et al., 2008), the developing Human Connectome Project (dHCP) pipeline (Makropoulos et al., 2018) and MATLAB R2022a.

dMRI processing was performed as follows: for each subject, the two dMRI acquisitions were first concatenated and then denoised using a Marchenko-Pastur-PCA-based algorithm (Veraart et al., 2016). eddy current, head movement and EPI geometric distortions were corrected using outlier replacement and slice-to-volume registration (Andersson et al., 2017, 2016, 2003; Andersson and Sotiropoulos, 2016), bias field inhomogeneity correction was performed by calculating the bias field of the mean b0 volume and applying the correction to all the volumes (Tustison et al., 2010). The DTI model was fitted in each voxel using the weighted least-squares method *dtifit* as implemented in FSL using only the b = 750 s/mm^2 shell.

Structural MRI (T1w and T2w) images were processed using the dHCP minimal processing pipeline to obtain the bias field corrected and coregistered T2w and T1w, brain masks, tissue segmentation and the different tissue probability maps (Makropoulos et al., 2018, 2014). Then T1w/T2w ratio maps were obtained using the bias field corrected images. The T1w/T2w maps were edited to remove voxels with intensities higher than the mean + 5 standard deviations. Note that a calibration step was not included, as the full dataset was scanned with the same parameters in the same scanner, minimising differences in intensity scale (Ganzetti et al., 2014).

2.3 Magnetisation transfer imaging processing

MTI data were processed as previously described (York et al., 2022b, 2020). The three echoes were summed together to increase the signal-to-noise ratio (SNR) (Helms and Hagberg, 2009) for each MT image (MT_{off}, MT_{on} and MT_{T1w}). MT_{on} and MT_{T1w} images were coregistered to the MT_{off} image using flirt (Jenkinson et al., 2002; Jenkinson and Smith, 2001). From (Helms et al., 2010b, 2008a) we can define the amplitude of the spoiled gradient echo at the echo time (App) as:

$$\frac{S_{T1w}}{S_{off}} = \frac{\left(1 - e^{-TR_{T1w}R_1}\right)\sin\alpha_{T1w}\left(1 - e^{-TR_{off}R_1}\right)\cos\alpha_{off}}{\left(1 - e^{-TR_{off}R_1}\right)\sin\alpha_{off}\left(1 - e^{-TR_{T1w}R_1}\right)\cos\alpha_{T1w}}$$

where S, TR and α represent the signal intensity, the repetition time (in seconds), and the flip angle (in radians), respectively. The subscript *off* stands for the proton density-weighted acquisition and the subscript *T1w* for T1-weighted image.

The R1app is expressed as:

$$MTR = \frac{M_0 - M_{on}}{M_0} \times 100$$

By combining R1app and Aapp, we can obtain the MTsat:

$$MTsat = \frac{\alpha \cdot TR \cdot R1app \cdot M_{on} - \alpha^2/2}{M_{on}}$$

where S_{on} represents the intensity signal of the magnetization transfer weighted image.

Finally, the MTR can be obtained as follows:

$$MTR = \frac{M_0 - M_{on}}{M_0} \times 100$$

2.4 Registration to a common space

MTsat and MTR maps were registered to the structural T1w (MPRAGE) images processed with the dHCP pipeline using ANTs symmetric normalisation (SyN) (Avants et al., 2008). The tissue probability maps for the grey matter (GM) and WM were obtained from the dHCP pipeline (Makropoulos et al., 2018). Nonlinear diffeomorphic multimodal registration was then performed between age-matched T2w and GM/WM tissue probability maps from the dHCP extended volumetric atlas (Fitzgibbon et al., 2020; Schuh et al., 2018) to the subjects T2w and GM/WM tissue probability using SyN (Avants et al., 2008). This was combined with the corresponding template-to-template transformation to yield a structural-to-template (40 weeks GA) transformation, which was finally combined with the MTsat-to-structural transformation to obtain the final MTsat-to-template alignment. By combining all the transformations, image registration was performed with only one interpolation step.

2.5 Tract-based spatial statistics

The mean b0 EPI volume of each subject was co-registered to their structural T2w volume using boundary-based registration (Greve and Fischl, 2009). This was combined with the structural-to-template transformation to create the diffusion-to-template transformation and propagate the FA maps to the template space.

The FA maps were averaged and used to create the skeleton mask. MTsat and MTR parametric maps were propagated to template space using the MTsat-to-template transformation and projected onto the skeleton (Smith et al., 2006).

2.6 White matter tracts of interest

3 É Ø Ô Å Å Î 7 - Ô Ò Á Ã Ô Ó × Å Ò Å Ç Å Î Å Ò Á Ô Å Ä É Î Å Á Ã È Ó Õ Â Ê (Vaher et al., 2022). Briefly, the tract masks were propagated from the ENA50 atlas (Blesa et al., 2020). These masks were used as sets of regions of interest (ROI) for seeding the tractography, creating the tracts in native diffusion space. Then, the tracts were binarised only including voxels containing at least 10% of the tracts and propagated to MTsat space by

combining the MTsat-to-structural and diffusion-to-structural transformations to calculate the mean values in each tract.

2.7 Statistical analysis

Tract-based statistical analyses were conducted in R (version 4.0.5) (R Core Team, 2022). We performed multivariate multiple linear regression analyses for all WM tracts, with the tract-average metric as the outcome and preterm status and GA at scan as the predictor variables. Preterm status is a categorical variable (preterm versus term), and GA at scan is continuous variable that describes É Î Æ Á Î Ô Ó . Adjustment for GA at scan is a standard convention in quantitative neonatal MRI studies because MRI features are dynamic during early life so differences in age at image acquisition is a potential source of confounding in groupwise analyses. The outcome variables as well as GA at scan were scaled (z transformed) before fitting the models, thus, the regression coefficients reported are in the units of standard deviations. P-values were adjusted for the false discovery rate (FDR) using the Benjamini-Hochberg procedure (Benjamini and Hochberg, 1995) across all MTI metrics separately for the effects of preterm birth and GA at scan, and independently for the comparative FA, RD and T1w/T2w ratio tract-based analyses. The WM tract results were visualised using ParaView (ParaView Developers, 2020) with standardised betas represented as the effect size.

Voxel-wise statistical analysis was performed using a general linear univariate model with PALM (Winkler et al., 2014). Two different contrasts were tested: correlation with GA at scan adjusting for preterm status, and term vs preterm comparison adjusting for GA at scan. Family-wise error correction (FWER), across modalities for MTI metrics (MTsat and MTR) and separately for the complementary FA, RD and T1w/T2w analyses (Winkler et al., 2016), and threshold-free cluster enhancement (TFCE) were applied with a significance level of $p<0.05$ (Smith and Nichols, 2009).

The distributions of MTI metrics, FA, RD and T1w/T2w ratio were compared using two-dimensional histograms of co-registered indexed voxels (RNifti and ggplot2::geom_bin2d packages in R) (York et al., 2022a) and voxel-wise correlation analyses between the metrics were performed with repeated measures correlation as implemented in the R package *rmcorr* (Bakdash and Marusich, 2017); this was performed in the WM tissue segmentation obtained from the dHCP pipeline (Makropoulos et al., 2018). Tract-wise correlation Ã Ï Å ÆÆ É Ã É Å Î Ô Ó × Å Ò Å Ã Á Ì Ã Õ Ì Á Ô Å Ä Õ Ó É Î Ç 0 Å Á Ò Ó Ï Î õ Ó Á Ã Ò Ï Ó Ó Á Ì Ì Ô Ò Á Ã Ô Ó × Á Ó Ã Á Ì Ã Õ Ì Á Ô Å Ä Â Ù Æ É Ò Ó Ô Ô Ò taking the average, and then back-Ô Ò Á Î Ó Æ Ï Ò Í É Î Ç Ô È Å Ö Á Ì Õ Å Ô Ï 0 Å Á Ò Ó (Corey et al., 1998).

3 Results

3.1 Sample characteristics

The study group consisted of 105 neonates: 83 participants were preterm and 22 were term-born controls. Participant characteristics are provided in Table 1. Among the preterm infants, 15 (18.1%) had bronchopulmonary dysplasia (defined as need for supplementary Ï Ø Ù Ç Å 6 Î weeks GA), 3 (3.6%) developed necrotising enterocolitis requiring medical or surgical treatment, 15 (18.1%) had one or more episodes of postnatal sepsis (defined as detection of a bacterial pathogen from blood culture, or physician decision to treat with Á Î Ô É Â É Ï Ô É Ã Ó Æ Ï Ò I υ Ä Á Ù Ó É Î Ô È Å *Staphylococcus* Ô Ï Æ Ç Ò blood or a negative culture but raised inflammatory markers in blood), and 2 (2.4%) required treatment for retinopathy of prematurity.

Table 1: Neonatal participant characteristics.

	term (n=22)	preterm (n=83)	p-value*
GA at birth (weeks)	39.57 (36.42 - 41.56)	29.48 (24.14 - 32.84)	n/a
Birth weight (grams)	3340 (2410 - 4295)	1334 (594 - 2380)	n/a
Birth weight z-score	0.167 (-2.295 - 1.970)	0.060 (-3.132 - 2.141)	0.632
GA at scan (weeks)	41.93 (40.00 - 46.14)	40.77 (37.84 - 45.84)	<0.001
M:F ratio	13:9	49:34	1

**The last column reports the p Ö Á Ì Õ Å Ó Ï Æ Ô È Å Ç Ò Ï Õ Ð Ä É Æ Æ Å Ò Å Î Ã Å Ó Ã Ï Í Ð Õ Ô Å Ä Ö Á Ò É Á Â Ì Å Ó Á Î Ä & É Ó È Å Ò õ Ó Å Ø Á Ã Ô Ô Å Ó Ô Æ Ï ò Ã Á Ô Å Ç Ï Ò É Ã Á Ì Ö Á Ò É values for a continuous variable and for male/female.*

3.2 Magnetisation transfer imaging metrics in association with gestational age at scan and preterm birth

The average MTsat and MTR maps for the term and preterm infants are shown in Figure 1A (see Supplementary Figure 1 for examples of individual participant maps). From visual inspection of the averaged maps, MTsat and MTR show similar values across the two groups, although preterm infants at TEA have lower MTsat values mostly in the frontal regions and higher MTR values in the central regions. Tract-averaged values for MTsat and MTR for term and preterm groups are provided in Supplementary Table 1 and visualised in Figure 1B. The highest MTsat values are observed in the corticospinal tract, whilst MTR is highest in the anterior thalamic radiation and cingulum cingulate, followed by the corticospinal tract. The lowest values for MTsat and MTR are observed in the inferior longitudinal fasciculus.

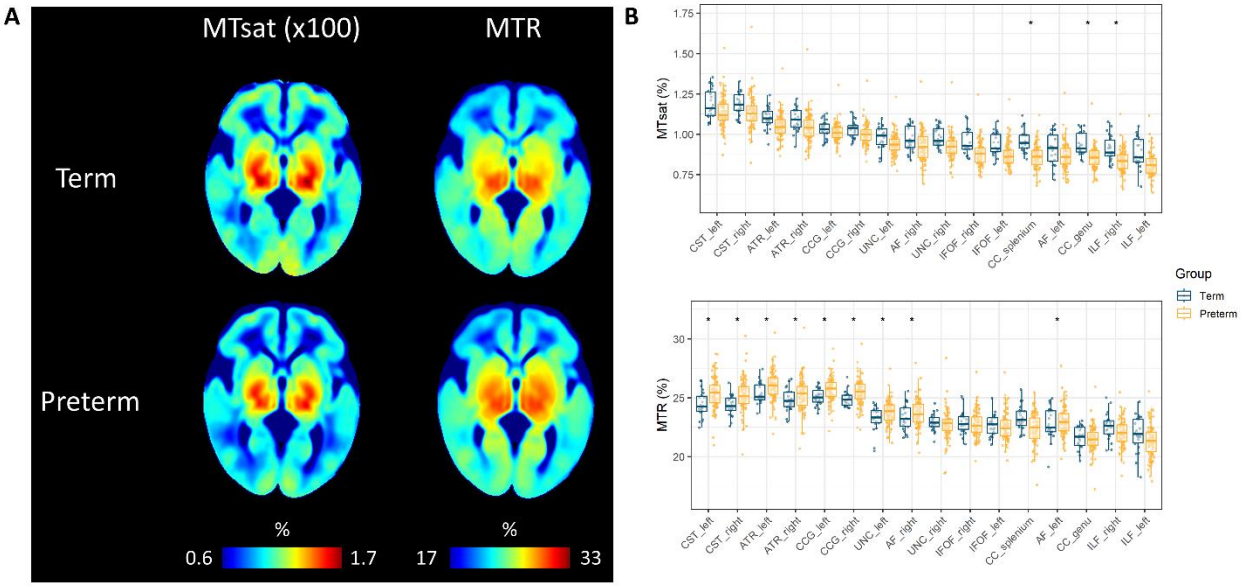

Figure 1:(A) Neonatal MTsat and MTR maps averaged across term and preterm subjects in the study. (B) Tract-averaged MTI metrics in the 16 white matter tracts; tracts are ordered by the values of MTsat. Asterisks (*) indicate tracts with statistically significantly different values between term and preterm infants. MTR = magnetisation transfer ratio, MTsat = magnetisation transfer saturation, CC genu = corpus callosum genu/forceps minor, CC splenium = corpus callosum splenium/forceps major, CST = corticospinal tract, IFOF = inferior fronto-occipital fasciculus, ILF = inferior longitudinal fasciculus, AF = arcuate fasciculus, UNC = uncinate fasciculus, CCG = cingulum cingulate gyrus, ATR = anterior thalamic radiation.

We used two complementary approaches to study the effect of GA at scan and preterm birth on the MTI metrics: voxel-wise in the WM skeleton, and ROI-based using mean values in 16 major WM tracts (Vaher et al., 2022).

MTsat and MTR are positively correlated with GA at scan within the neonatal period between 37-46 weeks of gestation after adjusting for preterm birth. These results were visible on both voxel-wise (Figure 2 left panel) and tract-based analyses (Figure 3 left panel). Positive correlations for both MTsat and MTR with GA at scan were observed when assessed separately in term and preterm groups (Supplementary Figure 2; Supplementary Tables 2-3).

Complementary analyses for DTI metrics showed positive correlations for FA and negative for RD with GA at scan across the WM skeleton (Supplementary Figure 3 left panel) and tracts (Supplementary Table 4). T1w/T2w ratio had statistically significant positive correlations with GA at scan in the majority of tracts, except in the arcuate fasciculus, corpus callosum and cingulum cingulate (Supplementary Table 4; Supplementary Figure 3 left panel). On average, GA at scan correlations with MTsat, MTR, FA and RD were of a similar Í Á Ç Î É Ô Õ Ä Å j á cross tracts (|0.524| - |0.589|), whilst correlation with T1w/T2w Ò Á Ô É Ï × Á Ó Ì Ï × Å Ò j Í Å Á Î r È π 8 ρ ω χ Q 8

Although we observed that both MTsat and MTR positively correlate with GA at scan, the effect of preterm birth was different for these two metrics. Compared to preterm infants, term infants had higher MTsat values in the genu and splenium of the corpus callosum (Figure 2 right panel). Tract-level analyses showed similar results (Figure 3 right panel). In contrast, MTR was higher in preterm infants, with significant differences in the central WM regions, and in the corticospinal tracts and uncinate fasciculi (Figure 2 and 3 right panels).

Complementary analysis of DTI metrics (Supplementary Figure 3 right panel, Supplementary Table 4) showed higher FA values in the term group, with the strongest effects observed in the genu and splenium of the corpus callosum and the uncinate. These higher values of FA in the term group were paralleled with lower values of RD. This accords with our previous findings in the wider cohort (Vaher et al., 2022). T1w/T2w ratio was significantly higher in the term group across the WM skeleton and the tracts (Supplementary Figure 3 right panel, Supplementary Table 4), with a Ì Á Ò Ç Å ÅÆÆÅÃÔ ÓÉÚÅ ¡ ÍÅÁÎ

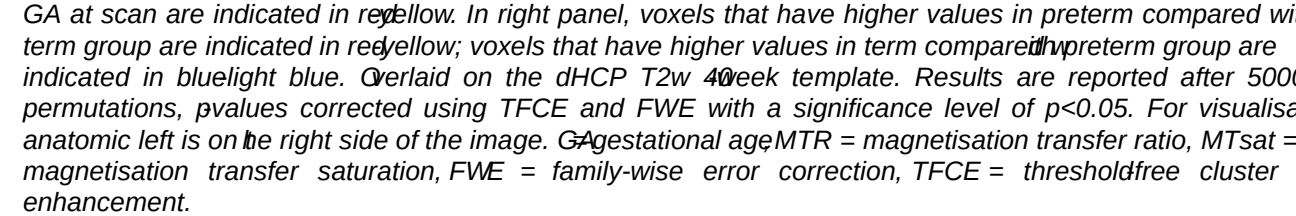

Figure 2: Voxel-wise analysis showing effects of GA at scan and preterm birth on magnetisation transfer imaging metrics. Models were mutually adjusted for GA at scan and preterm status. The first row represents the WM skeleton mask (green) where voxel values were compared. In left panel, voxels that have positive correlation with GA at scan are indicated in red-yellow. In right panel, voxels that have higher values in preterm compared with term group are indicated in red-yellow; voxels that have higher values in term compared with preterm group are indicated in blue-light blue. Overlaid on the dHCP T2w 40 week template. Results are reported after 5000 permutations, p-values corrected using TFCE and FWE with a significance level of p<0.05. For visualisation: anatomic left is on the right side of the image. GA = gestational age, MTR = magnetisation transfer ratio, MTsat = magnetisation transfer saturation, FWE = family-wise error correction, TFCE = threshold-free cluster enhancement.